Published by JScE as Proceedings of 4th International Conference on Earthquake Engineering and Post-Disaster Reconstruction Planning (ICEE-PDRP), 19-21 Jan. 2026, Bhaktapur, Nepal

DESIGN AND CALIBRATION OF A MEMS SEISMIC MONITORING SYSTEM

Abina Makaju[1]*, Rajani Shrestha[1], Rojishma Laghu[1], Shriya Chakatu[1], Subeg Man Bijukchhen[2], Yogesh Bajracharya[1]

[1] Department of Electronics and Communication Engineering, Khwopa Engineering College, PU
[2] PG Department of Earthquake Engineering, Khwopa Engineering College, PU

Abstract

We designed a seismic monitoring system integrating Micro Electro-Mechanical Systems (MEMS) accelerometer sensors with a Raspberry Pi and long-range (LoRa) communication technology. The system aims to provide a cost-effective and flexible approach for studying ground motion at various locations, with applications in geological research and disaster preparedness.Two types of MEMS sensors were employed to measure ground acceleration in three components. The Raspberry Pi functions as the central processing unit, responsible for data acquisition, processing, and storage. The data is saved in ASCII format and transmitted wirelessly to the main monitoring station using LoRa modules. Calibration of the system is carried out on a 1D shake table to ensure measurement accuracy. Further performance validation is conducted by comparing the sensor outputs with a standard strong-motion seismometer (Mitsutoyo JEP-6A3-2) in both the time and frequency domains. Experimental results from ambient vibration measurements indicate that the MPU6050 sensor achieves a higher goodness of fit with the strong-motion seismometer as compared to the ADXL345. This highlights the importance of filtering and calibration in improving measurement precision. Despite the limitations, the proposed system offers a scalable and cost-effective solution for seismic data collection of seismic monitoring system.

Keywords: Acceleration; LoRa; Cost-effective seismometer; MEMS; Raspberry Pi

1. Introduction

The Earth is in a state of constant motion, such as tectonic plates grinding, shifting, and colliding with great force resulting earthquakes that reshape the landscape and add threat to human communities. Seismic monitoring plays a foundational role as it delivers quantitative data on earthquake magnitude, the position of the epicenter, the quantity of seismic occurrences, and the characteristics of ground motion, all of which are useful for scientific research, hazard assessment and disaster mitigation strategies (Braille, 2018).

Nepal's location within the Himalayas' active collision zone makes it prone to seismic activity. The Government of Nepal has a network of 42 seismic stations, 50 GPS stations, and 36 accelerometers (Department of Mines and Geology, n.d.). Nevertheless, the network remains relatively inadequate when compared against more technologically advanced countries. For instance, Japan Meteorological Agency maintains a dense network of over 700 seismic intensity-meters, more than 300 seismometers and over 80 tsunami meters in their country.

Geophones have been used as the main sensing component of conventional seismometer but their effectiveness is hampered by significant limitations, including high costs, a sensitivity to environmental changes, and the critical requirement for direct physical connection to data gathering systems although they are robust and reliable (Hou et al., 2021).

Recent advancement in MEMS sensors and the Internet of Things (IoT) is revolutionizing the field of seismic monitoring. MEMS sensors are compact, low-cost, and energy-efficient, enabling large scale deployment, while IoT facilitates real-time data transmission and remote supervision. Furthermore, Long-range (LoRa) communication provides a low-power, reliable alternative

*Corresponding author: Abina Makaju
Department of Electronics and Communication Engineering, Khwopa Engineering College, Bhaktapur, Nepal
Email: abinamakaju@gmail.com
https://doi.org/10.3126/jsce.v13i1.89509

for remote or challenging terrains (Gad-el-Hak, 2005). By integrating these technologies, it is now possible to build dense, high resolution seismic networks that improve early warning systems, enhance disaster preparedness, and provide deeper insight into earthquake dynamics.

2. Literature Review

Early earthquake monitoring and hazard management systems primarily relied on broadband sensors. While these instruments provided reliable and accurate data, they were bulky, expensive, and limited in terms of widespread deployment. These limitations created the need for compact and cost-effective alternatives (Naik et al., 2007).Recent studies highlight the increasing use of Micro-Electro-Mechanical Systems (MEMS) accelerometers as low-cost seismic sensors. Projects such as the QuakeCatcher Network and MyShake demonstrated the feasibility of using MEMS accelerometers for real-time earthquake detection. Their low cost and versatility make them suitable for dense urban deployments, bridging gaps in station coverage (Wu & Mittal, 2021).

Beyond accelerometer-based approaches, GPS has been investigated as a seismic monitoring tool (Weijun & Gang, 2008) for capturing crustal movement, identifying earthquake precursors, and analyzing post-seismic deformation. It shows potential of using GPS for earthquake forecasting and hazard assessment, particularly for mid- and long-term monitoring.The integration of IoT frameworks with MEMS accelerometers opened new avenues for seismic monitoring. There has been attempt of using MEMS accelerometers with NodeMCU for real time earthquake monitoring (Pandey et al., 2021). Another setup using ADXL335 accelerometers integrated with Arduino successfully detected and transmitted P-wave signals while incorporating retransmission protocols for error handling (Priyana et al., 2017). However, the limited processing capability of NodeMCU warrants more powerful units such as Raspberry Pi, enabling faster computation and user-friendly graphical interfaces.

Sapkota et al. (2024) combined MEMS accelerometers, Raspberry Pi, GPS synchronization, and LoRa communication to enable real-time seismic monitoring and inter-station data sharing.A low-cost system using MPU-6050 with microcontrollers successfully differentiated seismic and non-seismic vibrations but suffered from false positives and reduced sensitivity compared to professional seismometers (Perwej et al., 2022). A study comparing ADXL345 and MPU-6050 accelerometers found MPU-6050 to be more consistent and reliable under random vibrational inputs (Rodrigues et al., 2021). Use of MPU-6050 with Arduino for a low-cost seismometer capable of filtering seismic frequencies (0.625–5 Hz), computing RMS acceleration, and logging real-time data has also been carried out (Pavleski, 2019).

The review of past literature demonstrates a substantial progress in low-cost seismic monitoring and early warning systems. MEMS accelerometers, when combined with IoT platforms, GPS synchronization, and advanced processing units, have shown significant potential for both research and practical deployment. Nonetheless, existing systems often face challenges such as limited sensitivity, slower processing speeds, and false-positive detections.

Building on these insights, the proposed work aims to develop a scalable and affordable seismic monitoring system that leverages the processing power of Raspberry Pi, robust communication protocols, and accurate MEMS sensors. The system will focus on improving real-time data execution, reliability, and usability, making it suitable for both academic research and practical hazard mitigation.

3. Methodology

The procedure that is applied for the development of effective seismic monitoring system is given by the following steps:

3.1. Working Principle

The setup used two MEMS accelerometers, ADXL345 and MPU6050. These sensors contain tiny movable and fixed plates that form capacitors. When acceleration is experienced, the movable plate shifts, altering the capacitance, which is then converted into an electrical signal representing three-axis acceleration. This signal is transmitted to the Raspberry Pi through the I^2C interface, making the configuration suitable for seismic monitoring. The raw value output from the accelerometer can be converted to acceleration in g units by dividing the raw output by the sensor's sensitivity (Equation 1).

$$\text{Acceleration (g)} = \frac{\text{Raw sensor output}}{\text{Sensitivity (LSB/g)}} \tag{1}$$

where,
Raw Sensor output is the 16-bit signed integer output from the MEMS. Sensitivity refers to how much the output digital value changes in response to a change in acceleration in Least Significant Bits (LSB) per g.

$$1\text{g} = 9.81 \text{ m/sec}^2 \tag{2}$$

Considering seismic responses involve low-amplitude vibrations, the raw acceleration readings from the MEMS accelerometer are converted into cm/s^2 through data processing in the Raspberry Pi. Accordingly, the modified equation for acceleration can be written as in Equation 2.

$$\text{Acceleration (cm/s}^2) = \text{Acceleration (g)} \times 981 \tag{3}$$

where,
Acceleration (g) is the value of acceleration in terms of g-units recorded in accelerometer. $1m/s^2 = 100cm/s^2$

The converted acceleration data, along with the corresponding time information, is stored in an external memory unit and simultaneously transmitted to the receiver module for remote recording. A block diagram of the complete system comprising both transmitter and receiver is shown in Figure 1.

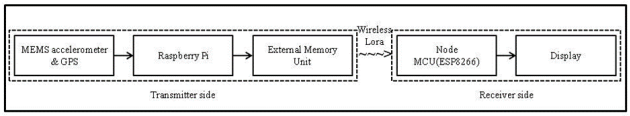

Figure 1. Block diagram of seismic monitoring system

3.2. Calibration Using Reference Seismometer

Figure 2. Seismometer setup for measurement and calibration

The MEMS accelerometer based seismic monitoring system was setup alongside a strong motion seismometer (Mitsuyo JEP-6A3-2) at Khwopa Engineering College for calibration. The accelerometer's X-axis and Y-axis were kept point North and East respectively and Z-axis was oriented perpendicular to the horizontal plane to monitor ambient ground vibrations or microtremors.

The acceleration readings from both systems were compared to evaluate the accuracy and reliability of the MEMS system. Consistency between the MEMS and reference seismometer ensures that the system was reliable. In case of significant differences, the MEMS system has to be re-calibrated to make sure that measurements were always accurate and consistent. The hardware setup of the system alongside the reference seismometer is shown in Figure 2.

The workflow of the proposed MEMS based seismic monitoring system is illustrated in Figure 3. The system starts up and constantly monitors vibrations and records the acceleration and time. The recorded data are always saved locally and also sent to a monitoring station through LoRa whenever the network is available. After that, the readings are compared to data from a reference seismometer, and the system is re-calibrated if necessary. When the readings are consistent, the system is fully calibrated and made ready for reliable monitoring.

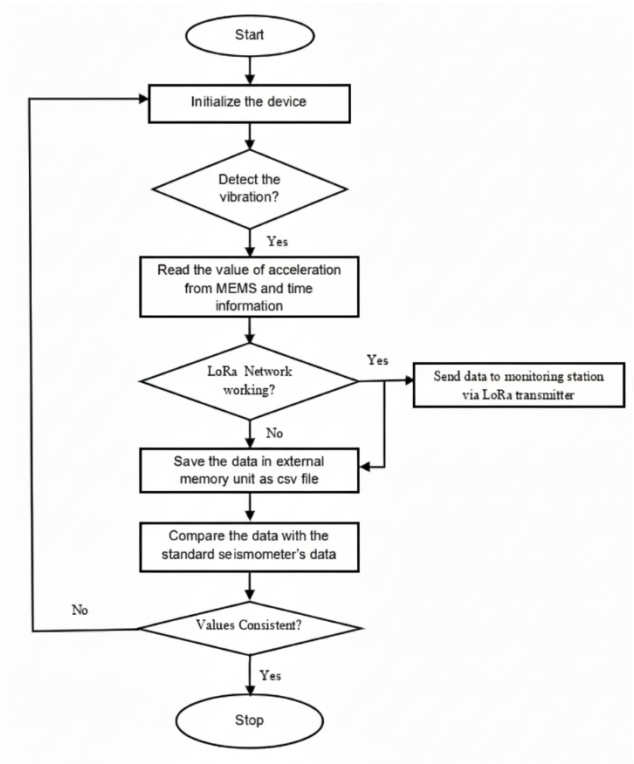

Figure 3. Flowchart of the overall system

4. Results and Discussion

The results obtained from the analysis are discussed in detail as follows.

4.1. Comparison Between MEMS Accelerometer ADXL345 and Strong-motion Seismometer (Mitsuyo JEP-6A3-2) in Frequency Domain

Figure 4 represents the frequency spectrum of acceleration data, comparing the results from MEMS seismic monitoring system (based on Raspberry Pi and ADXL345) to that of the Mitsutoyo JEP-6A3-2 acclerometer in the frequency domain. The horizontal axis represents the frequency components of the measured microtremors while the vertical axis represents amplitude, with values ranging from 0 Hz to 35 Hz. In order to observe the amplitude value difference and fluctuations for the frequency amplitude of ADXL345 and JEP-6A3-2 properly, we zoomed the Figure 4 as Figure 5.

In Figure 5, some part of the amplitude value difference

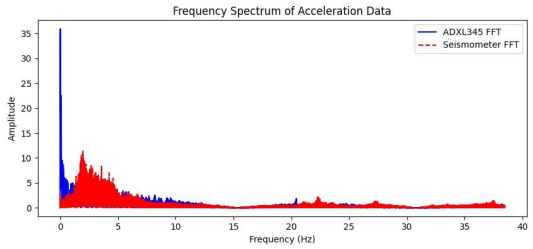

Figure 4. Frequency spectra of acceleration data (ADXL345)

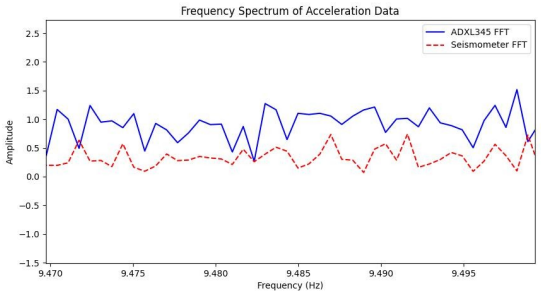

Figure 5. Zoomed section of frequency spectra of acceleration data (ADXL345)

and fluctuations are observed for the ADXL345 FFT and Seismometer FFT. These variations can be attributed to variances in sensor sensitivity, frequency response, noise susceptibility, calibration, and installation process. These factors collectively lead to variations in how each system captures and represents the microtremors, despite being placed in the same location.

4.2. Comparison Between MEMS Accelerometer ADXL345 and Strong-motion Seismometer (Mitsutoyo JEP-6A3-2)

Figure 6 is a log-log plot of the frequency spectra, comparing the data from seismic monitoring system (using Raspberry Pi and ADXL345) with that from a standard seismometer.

The log-log graph is plotted as it is powerful tool for analyzing seismic data, especially microtremors, as it allows for clear visualization of a wide range of frequencies and amplitudes.

The data is plotted on logarithmic scales for both amplitude (y-axis) and frequency (x-axis). The horizontal axis represents the frequency components of the measured ambient vibrations, ranging from 0.001 Hz to 10 Hz. The vertical axis represents the amplitude components on a logarithmic scale.

Figure 6 shows that the spectral amplitude of ADXL345

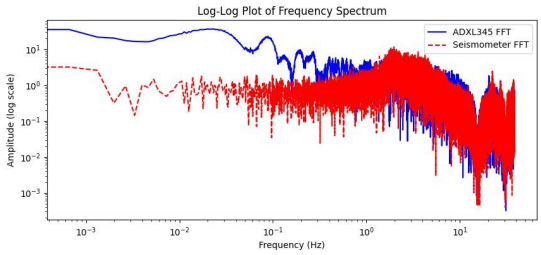

Figure 6. log-log plot of frequency spectrum (ADXL345)

and JEP-6A3-2 differ mostly due to variances in sensor sensitivity, frequency response, noise susceptibility, calibration, and mounting. Despite being installed at same locations, these factors combine to cause variances in measurement. The log-log plot highlights these differences and gives useful information about the nature of seismic noise or ambient vibration.

To filter out the noise, a Butterworth low-pass filter is applied. The filter is characterized by its maximally flat frequency response in the passband, meaning it does not introduce ripples and preserves the true amplitude of signals below the cutoff frequency. The 5th order Butterworth filter is used to obtain Figure 7.

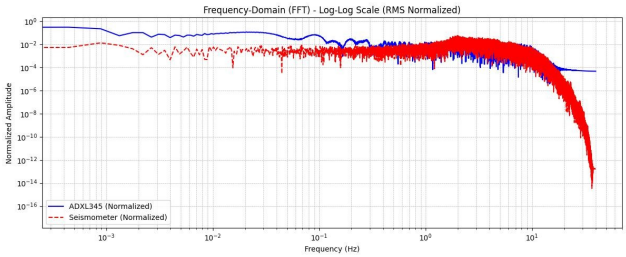

Figure 7. Log-log plot of frequency spectra after filtration (ADXL345)

The Butterworth filter had effectively suppressed amplitude content below because of which the shows more comparable normalized amplitudes, with the seismometer maintaining a lower noise floor. The flattening of the ADXL345 curve at very low frequencies indicates potential sensor or environmental noise that persists even after filtering.This plot demonstrates how filtering enhances signal clarity and helps in assessing the low-frequency performance of low-cost sensors like the ADXL345 relative to scientific-grade equipment. For the more detail view of filtered-out data, the Figure 7 is zoomed to give Figure 8. This shows that the ADXL 345 can still capture meaningful low-frequency data after proper filtering and normalization.

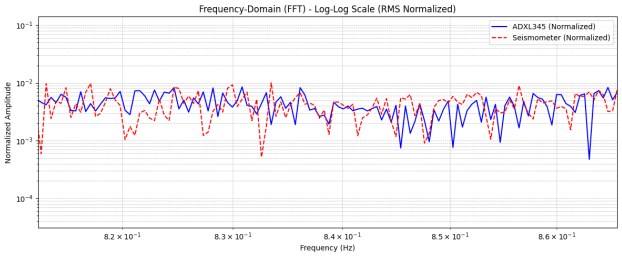

Figure 8. Zoomed log-log plot of frequency spectrum after filtration (ADXL345)

4.3. Comparison Between MEMS Accelerometer MPU6050 and Strong-motion Seismometer (Mitsutoyo JEP-6A3-2) using FFT Plot

In this study, the performance of seismic monitoring system using the MPU6050 accelerometers is compared with strong-motion seismometer (Mitsutoyo JEP-6A3-2). This comparison is conducted by replacing the ADXL345 with the MPU6050 under the same process as used with the ADXL345-based system.

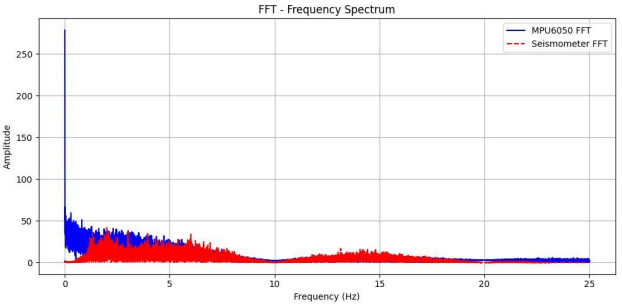

Figure 9. Frequency spectrum of acceleration data (MPU6050)

Figure 9 shows the frequency spectra of acceleration data, comparing those from seismic monitoring system (based on Raspberry Pi and MPU6050) and strong-motion seismometer JEP-6A3-2.

This shows there is variation between spectra of MPU6050 and that of JEP-6A3-2.

4.4. Comparison Between MEMS Accelerometer MPU6050 and JEP-6A3-2 using Log-log Plot of Frequency Spectrum

For ambient vibration or seismic studies, the most informative signals often exist in the low-frequency, low-amplitude range. A linear frequency spectra may hide small but meaningful variations, when high-amplitude noise is dominant. Therefore, a log-log plot on the amplitude axis helps expand small values, making it easier to detect signal differences for accurate analysis. Figure 10 is frequency spectra in log-log, comparing the data from seismic monitoring system (using Raspberry Pi and MPU6050) with a strong motion seismometer. Figure 11 shows zoomed version of the Figure 10.

This zoomed plot shows that the MPU6050 exhibits consistently higher amplitude across the frequency range than the strong motion seismometer, indicating greater noise or sensitivity in its signal. This slight difference can be attributed to sensor noise, environmental factors, or inherent limitations of the MPU6050 sensor. Further calibration or noise filtering techniques could help reduce this variability in future iterations. A low-pass filter is applied to remove the aforementioned noise (Figure 12).

The filtering has improved the signal quality and we can extract meaningful low frequency parts from it. This filter helps isolate the low frequency components relevant to seismic activity by removing unwanted high frequency noise caused by mechanical vibrations and sensor limitations. For the further analysis, Figure 12 is zoomed in section around 3Hz (Figure 13).

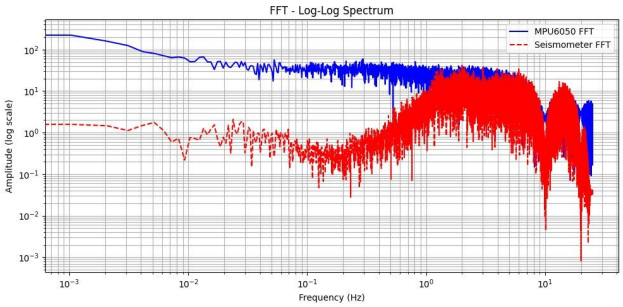

Figure 10. Log-log plot of frequency spectrum (MPU6050)

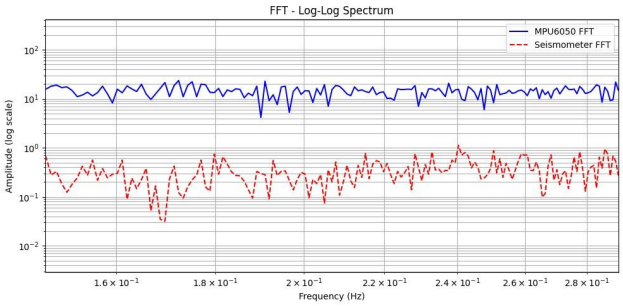

Figure 11. Zoomed log-log plot of frequency spectrum (MPU6050)

It also improves the clarity of the FFT results enhancing comparability with a reference seismometer and reducing the chances of false event detection. This filtering step is essential to ensure reliable analysis from the low-cost sensor.

4.5. Statistical Analysis of Sensor Performance

In addition to frequency-domain analysis, statistical comparison is carried out between the measurements

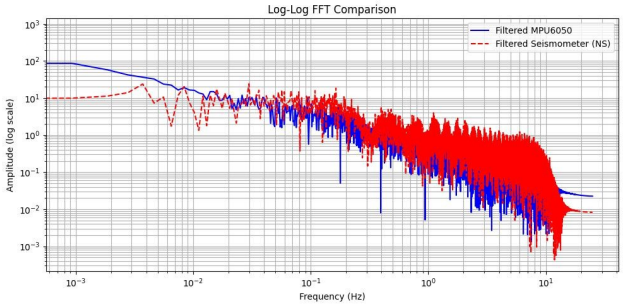

Figure 12. Log-log plot of frequency spectrum after filtration (MPU6050)

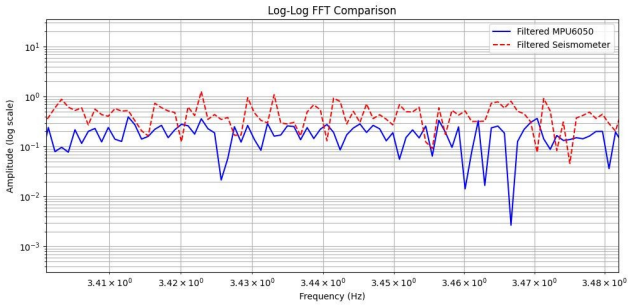

Figure 13. Zoomed log-log plot of frequency spectrum after filtration (MPU6050)

from our system (MPU6050 & ADXL 345) against the standard reference system (strong-motion seismometer) after filtration. The analysis focused on variance, goodness of fit, and correlation coefficient to quantify how closely the MEMS sensors replicate the standard reference measurements.

Case I (MPU6050)
This test evaluates the performance of the MPU6050 accelerometer in comparison to a standard strong motion sensor (JEP-6A3-2) under identical conditions. The results from our system using MPU6050 is represented as X and that from the strong-motion system is represented as Y in Table 1.

Table 1. Comparison of Statistical Parameters for MPU6050 and JEP-6A3-2

Parameter	MPU6050 (X)	JEP-6A3-2 (Y)
Mean	0.4376	0.2491
Median	0.4971	0.2113
Standard Deviation	10.1440	12.2353
Variance	102.9015 (S_{xx})	149.7026 (S_{yy})

$$\begin{aligned}\text{Variance (residual)} &= S_{xx} - S_{yy}\\ &= 149.7026 - 102.9015\\ &= 46.8011\end{aligned}$$

$$\begin{aligned}R^2\text{(Goodness of fit)} &= 1 - \frac{Var(Residual)}{S_{yy}}\\ &= 1 - \frac{46.8011}{149.7026}\\ &= 0.6873 \approx 68.73\%\end{aligned}$$

$$\text{Correlation Coefficient (r)} = \sqrt{0.6873} = 0.8290$$

In Case 1, our system with MPU6050 exhibited a variance of 102.9015, compared to the strong-motion system (JEP-6A3-2)'s variance of 149.7026. Using a simplified residual variance model, we calculated the goodness of fit (R^2) to be approximately 68.73% of the similar reading as that of the standard one reading.

Test Case II (ADXL345)
This test assesses the performance of the ADXL345 accelerometer compared to JEP-6A3-2 under identical vibration conditions. Data from our system with ADXL345 is indicated as X those from JEP-6A3-2 as Y (Table 2).

Table 2. Comparison of Statistical Parameters for ADXL345 and JEP-6A3-2

Parameter	ADXL345 (X)	JEP-6A3-2 (Y)
Mean	0.0042	0.0006
Median	-0.0235	0.0018
Standard Deviation	0.6531	0.5511
Variance	0.4266 (S_{xx})	0.3037 (S_{yy})

$$\begin{aligned}\text{Variance (residual)} &= S_{xx} - S_{yy}\\ &= 0.4266 - 0.3037\\ &= 0.1229\end{aligned}$$

$$\begin{aligned}R^2\text{(Goodness of fit)} &= 1 - \frac{Var(Residual)}{S_{yy}}\\ &= 1 - \frac{0.1229}{0.3037}\\ &= 0.5953 \approx 59.53\%\end{aligned}$$

$$\text{Correlation Coefficient (r)} = \sqrt{0.5953} = 0.7715$$

Similarly, for case 2, our system (ADXL345) exhibited a variance of 0.4266 compared to 0.3037 of the strong-motion system. Then, applying the same estimation method, we calculated the goodness of fit (R^2) to be approximately 59.53% of the similar reading as that of the standard one reading. Hence, based on the statistical analysis, it

can be seen that the MPU6050 has a higher goodness of fit ($R^2 = 0.6873 \approx 68.73\%$) than the ADXL345 ($R^2 = 0.5953$ or 59.53%) when compared to a standard strong-motion seismometer (JEP-6A3-2). We can conclude that the MPU6050 provides more reliable and consistent measurements than the ADXL345, which means our first test setup (MPU6050) performed better than the second test setup (ADXL345) in terms of alignment with a standard strong-motion system.

4.6. Gaussian Probability Density Function for X-Axis

Figure 14 and Figure 15 compare the amplitude distribution of acceleration along the X-axis between our system (MPU6050 sensor) and JEP-6A3-2 using Gaussian Probability Density Functions (PDFs). The blue curve represents the filtered signal from the MPU6050, while the red represents the signal from the standard strong motion system.

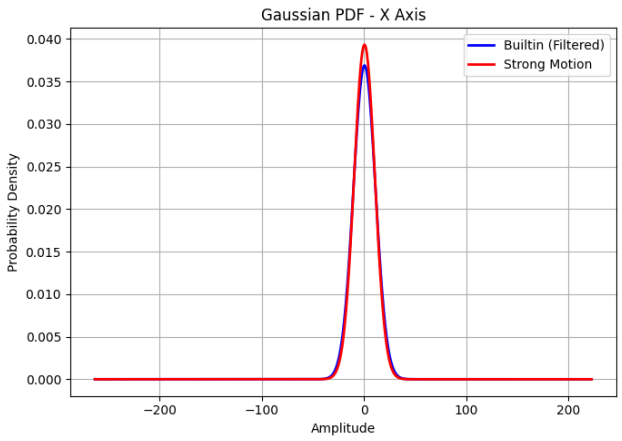

Figure 14. Gaussian Probability Density Function for X-axis using MPU6050

In Figure 14 and Figure 15, both curves show a sharp peak centred around zero, indicating that the signals are normally distributed with most of the amplitude values clustered near the mean. The close alignment of the two curves suggests that the built-in MPU6050 sensor provides a distribution similar to the standard reference, particularly in terms of amplitude variation and consistency along the X-axis. This strong overlap supports the conclusion that the MPU6050 sensor delivers reliable measurements in this direction.

In Figure 14 and Figure 15, the two curves exhibit similar bell-shaped distributions centered near zero on X-axis, indicating that both datasets follow a near-normal distribution. However, the red curve (standard strong motion) has a slightly higher peak and narrower spread, suggesting less variation in amplitude. The ADXL345 curve

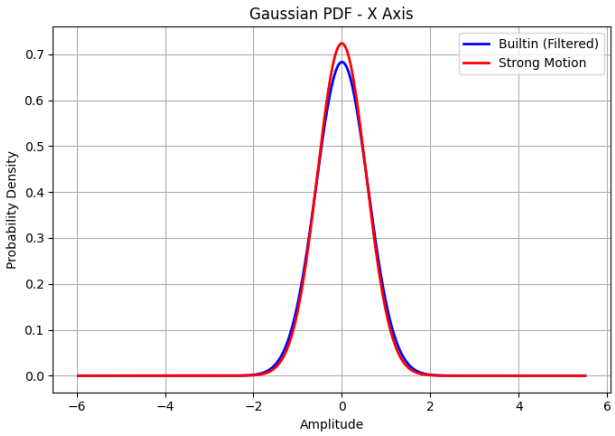

Figure 15. Gaussian Probability Density Function for X-axis using ADXL345

shows a broader spread, indicating slightly more noise or variability in the sensor's signal. This slight deviation shows that ADXL345 can perform reasonably but it introduces more signal variation compared to the strong motion system.

Therefore, this confirmed that MPU6050 provides more consistent seismic data than ADXL345.Overall, while distance plays a small role in increasing delay, the main reasons are protocol features, processing time, buffering, and system-level latency remain consistent across all test scenarios.

5. Conclusion

The proposed seismic monitoring system offers a cost-effective and scalable approach to ground motion measurement. By integrating MEMS accelerometers with a Raspberry Pi and LoRa communication, the system ensures reliable data acquisition, storage, and remote transmission. Acceleration data, stored in CSV format, can be easily analyzed for seismic studies, while real-time visualization through a local server enhances monitoring and decision-making capabilities. Experimental results confirm that the device is well-suited for deployment in dense seismic networks, contributing to both earthquake research and disaster preparedness.

References

Braille, L. W. (2018, April). Braille book review, march-april 2018. https://www.loc.gov/nls/new-materials / braille - book - review / braille - book - review-march-april-2018/

Department of Mines and Geology. (n.d.). National earthquake monitoring and research center [Retrieved from Department of Mines and Geology].

Gad-el-Hak, M. (2005). *Mems: Applications*. CRC press.

Hou, Y., Jiao, R., & Yu, H. (2021). Mems based geophones and seismometers. *Sensors and Actuators A: Physical*, *318*, 112498.

Naik, T. B. R., Saha, S., Raghavan, R., & Sarma, A. (2007). Modern seismic monitoring systems for earthquake hazard managementand mitigation. *IETE Technical Review*, *24*(3), 153–162.

Pandey, N., Rao, K. H. S., Seshank, V., Pokala, S., & Sunil, A. T. (2021). Earthquake alert system based on iot technology. *JETIR*.

Pavleski, M. (2019, October 31). *Sensitive mpu6050 seismometer with data logger*. Retrieved January 6, 2026, from https://www.hackster.io/mircemk/sensitive - mpu6050 - seismometer - with - data - logger-9e6bf5

Perwej, Y., Jitendra, Yadav, A. K., Rawat, V., & Divya, K. (2022). A system for monitoring seismic activity based on internet of things (iot). *International Journal of Modern Engineering Research*, *11*(7(1)). https : / / ijmer . in / issues / volume11 / volume11-issue7(1).aspx

Priyana, Y., Laumal, F. E., & Husni, E. (2017). Development of earthquake early warning system using adxl335 accelerometer. *Proc. Int. Conf. Satell. Technol*, 81–85.

Rodrigues, J. V. O., Pedroso, M. P. G., Silva, F. F. B., & Junior, R. G. L. (2021). Performance evaluation of accelerometers adxl345 and mpu6050 exposed to random vibrational input. *Research, Society and Development*, *10*(15), e286101523082–e286101523082.

Sapkota, Y., Tamrakar, R., Khadka, R., Yadav, A., Bijukchhen, S. M., & Bajracharya, Y. (2024). Design and testing of low-cost mems accelerometer on 1d shake table. *Journal of Science and Technology*, *4*(2), 71–75.

Weijun, S., & Gang, L. (2008). Research of gps technology in seismic monitoring system.

Wu, Y.-M., & Mittal, H. (2021). A review on the development of earthquake warning system using low-cost sensors in taiwan. *Sensors*, *21*(22), 7649.